Biogeosciences Discuss., 11, 5811–5868, 2014
www.biogeosciences-discuss.net/11/5811/2014/
doi:10.5194/bgd-11-5811-2014

Biogeosciences Discussions Open Access

Insights into biogeochemical cycling from a soil evolution model and long-term chronosequences

M. O. Johnson[1], M. Gloor[1], M. J. Kirkby[1], and J. Lloyd[2]

[1]School of Geography, University of Leeds, Leeds, LS2 9JT, UK
[2]Department of Life Sciences, Imperial College London, Silwood Park Campus, Ascot, UK

Received: 27 February 2014 – Accepted: 31 March 2014 – Published: 23 April 2014

Correspondence to: M. O. Johnson (m.o.johnson@leeds.ac.uk)

Published by Copernicus Publications on behalf of the European Geosciences Union.

Abstract

Despite the importance of soil processes for global biogeochemical cycles, our capability for predicting soil evolution over geological timescales is poorly constrained. We attempt to probe our understanding and predictive capability of this evolutionary process by developing a mechanistic soil evolution model, based on an existing model framework, and comparing the predictions with observations from soil chronosequences in Hawaii. Our soil evolution model includes the major processes of pedogenesis: mineral weathering, percolation of rainfall, leaching of solutes, surface erosion, bioturbation and vegetation interactions and can be applied to various bedrock compositions and climates. The specific properties the model simulates over timescales of tens to hundreds of thousand years are, soil depth, vertical profiles of elemental composition, soil solution pH and organic carbon distribution. We demonstrate with this model the significant role that vegetation plays in accelerating the rate of weathering and hence soil profile development. Comparisons with soils that have developed on Hawaiian basalts reveal a remarkably good agreement with Na, Ca and Mg profiles suggesting that the model captures well the key components of soil formation. Nevertheless, differences between modelled and observed K and P are substantial. The fact that these are important plant nutrients suggests that a process likely missing from our model is the active role of vegetation in selectively acquiring nutrients. This study therefore indirectly indicates the valuable role that vegetation can play in accelerating the weathering and thus release of these globally important nutrients into the biosphere.

1 Introduction

Soils play a major role in many global biogeochemical cycles due to their position at the interface between the atmosphere and lithosphere. For example, soils influence the flow of water to rivers and vegetation, they govern the flux of nutrients between the lithosphere, vegetation and rivers and are also a source and sink of gases to the

atmosphere. A quantitative description of the evolution through time of the processes and properties within soils is therefore of great interest.

This study is motivated by several important global-scale questions. An example being the long-term carbon cycle, specifically the relationship between silicate mineral weathering and atmospheric CO_2 concentrations. Over multi-million year timescales atmospheric CO_2 concentrations are governed by the balance between silicate mineral weathering and CO_2 outgassing from volcanic and tectonic activity (Urey, 1952). Increased levels of atmospheric CO_2 promote the weathering of silicate minerals, which in turn, indirectly consumes atmospheric CO_2 (Walker et al., 1981). This weathering process which occurs within soils is also affected by many other factors such as temperature, precipitation, pH, soil depth and vegetation dynamics. The influence of each of these factors is hard to quantify from field studies alone and current modelling attempts lack true process-based weathering feedbacks within soil profiles. Another important Earth system process is the exchange of plant nutrients between the soil and vegetation, of particular importance is phosphorus which is almost completely derived from the lithosphere and considered a limiting nutrient for many tropical forests across the globe (Vitousek and Sanford Jr, 1986; Vitousek et al., 1993; Quesada et al., 2012).

Over recent years a range of chemical and physical soil chronosequence data, a valuable means of evaluating our understanding of evolutionary processes in soil profiles, has become available. A good example is the soils which have developed on the lava flows of Hawaii (e.g. Chadwick et al., 1999; Porder et al., 2007). However, to our knowledge, efforts to make complete use of these soil data sets and synthesise them within one consistent, process-based modelling framework have been limited.

Existing models of pedogenic processes are largely aimed at understanding landscape scale processes (Yoo and Mudd, 2008; Minasny and McBratney, 2001, 1999; Dietrich et al., 1995) and mainly focus on rates of soil production and pay less attention to biogeochemical processes occuring within the soils. Models developed to study whole profile evolution include those of Vanwalleghem et al. (2013); Cohen et al. (2010); Salvador-Blanes et al. (2007), which, like this study attempt to model the evo-

lution of soil resulting from exposed bedrock over geological timescales. These models track the vertical profile of particle size distribution through time by implementing a depth dependent soil production rate, chemical and physical weathering and overturning due to bioturbation. However, these models do not include a liquid phase so chemical processes or losses from the profile due to leaching are greatly simplified.

Soil models which do include such biochemical processes exist but these attempts generally focus on very specific microscale processes such as mineral dissolution and/or vegetation interactions and are not designed for understanding pedogenic processes (Goddéris et al., 2006; Wallman et al., 2005; Warfvinge and Sverdrup, 1992). An attempt to couple such processes with a pedogensis model is the SoilGen1 model (Finke and Hutson, 2008). This model simulates the evolution of nutrient, carbon and pH profiles, however, the model requires a large number of soil properties for initialisation and can thus only predict changes in existing soil profiles.

The model which on conceptual grounds we view as having the most potential for our purposes is the pedogenesis model developed by Kirkby (1985). This model is recognised as a pioneering attempt to model biogeochemical soil processes in the context of understanding hillslope processes (Hoosbeek and Bryant, 1992; Minasny et al., 2008). The model meets the criteria of being based upon physical processes, yet is sufficiently simple to allow the mechanisms and feedbacks behind the resulting properties to be understood.

The purpose of this paper is to introduce a soil evolution model based on the framework described in Kirkby (1985) and explore how well this updated model can reproduce current soil properties, by placing a strong emphasis on evaluation with data. Specifically we will demonstrate how the model can be used to further our understanding of long-term nutrient cycles.

In addition to the processes in the original model, we have included a more detailed representation of vegetation interactions with the soil. This includes vertical mixing and decay of organic carbon and CO_2 production, and uptake and return of plant nutri-

ents. We also simulate the weathering and transport of individual soil mineral elements opposed to the one soil *entity* described in Kirkby (1985).

In this paper we describe with equations the individual processes and mathematical basis of the updated soil evolution model. Following on from the model description, the basic performance of the model is explored. This demonstration of the model's capability is based on a hierachy of model simulations starting with a profile subject to weathering and leaching only, with each further simulation including an additional process. We then evaluate the model with soil chronosequence data from Hawaii, demonstrating what we can learn from such a model. The focus here is on soils of tropical systems, however, the model could potentially be applied to other biomes by adjusting the appropriate input parameters.

2 Model description

The process of soil evolution is conceptualised as a vertical profile of bedrock which undergoes both chemical and physical weathering resulting in an altered profile which we term soil. The formation of soil begins when water percolates into bedrock and initiates mineral dissolution. Chemical weathering in the model is based on the central assumption that dissolution equilibrium is reached between the rock minerals and percolating water (Kirkby, 1977, 1985). In the model, water acts directly on the elemental oxides of the parent material rather than on rock minerals. The oxide composition and density of the bedrock provides the intial conditions for the modelled weathering process.

The simulated percolation of rainfall through the profile provides the mechanism and rate for losses of dissolved ions from the soil layers. The modelled soil may deepen as a result of steadily increasing percolation through the profile resulting from the increasing pore space which is created by the leaching of dissolved rock oxides and also by the redistribution of soil by bioturbation and from direct removal by vegetation.

The specific soil properties the model predicts are: soil depth, pore space, the proportion of the initial elemental oxides remaining in each soil layer, pH of the soil so-

lution, organic carbon and pore CO_2 concentration. The processes included in the model are, chemical weathering of bedrock elements, percolation of rainwater, leaching of weathering products, surface erosion, bioturbation, plant litter decomposition and vertical transport, CO_2 production and diffusion and nutrient cycling. As well as chemical weathering, other adopted processes from Kirkby (1985) include losses of solutes via leaching, surface erosion, biological mixing and ionic diffusion. The model differs by keeping the bedrock elements separate throughout model calculations. Keeping chemical elements separate allows us to explore more comprehensively the individual cycling and feedbacks of important elements. The model processes are detailed in the following sections.

2.1 Mineral weathering and leaching

2.1.1 Equilibrium reactions

As already indicated, the model assumes that dissolution equilibrium is reached between the rock oxides and the percolating waters. Although a simplistic assumption, as a first order approximation, this is preferable to a formulation using kinetic dissolution equations which are particularly difficult to constrain due to the requirement of reactive mineral surface areas. Studies have also shown that the unknowns associated with kinetic reactions are very large, with weathering rates of minerals such as plagioclase behaving closer to equilibrium predictions in natural systems than to kinetic rates derived from experimental studies (White et al., 2001, 2008). The methods of calculating the equilibrium composition and thus the dissolution of rock oxides and subsequent pH of the soil solution are derived from Kirkby (1977) and Garrels and Christ (1965) and an example taken from Kirkby (1977) for SiO_2 is shown in the Appendix. The concentration of H^+ in solution can be calculated by balancing the charge of the solution. Many of the anions present in a soil solution result from the reactions with dissolved CO_2. These anions are calculated using the partial pressure of CO_2 in the soil air. The dominant anions in the soil water are $[HCO_3^-]$, $[OH^-]$ and $[CO_3^{2-}]$ and the relevant charge balance

equation for our modelled soil solution is thus

$$[H^+] + [Al(OH)_2^+] + 3[Al^{3+}] + [Na^+] + [K^+] + 2[Ca^{2+}] + 2[Mg^{2+}] + 3[Fe^{3+}] + 2[Fe^{2+}] = [HCO_3^-] + [OH^-] + 2[CO_3^{2-}] + [Al(OH)_4^-] + [H_3SiO_4^-] + 2[HPO_4^{2-}] \quad (1)$$

from which $[H^+]$ is calculated using a bisection method. The pH of the soil solution is thus determined by the partial pressure of CO_2 in the soil and dissolved ion concentrations.

The model assumes that the behaviour of the elemental oxides depends only on their relative composition in the bedrock. However, these oxides are not usually present on their own, but are instead constituents of more complex silicate minerals. This will alter the solubility of the individual oxides and to account for this Kirkby (1977) proposed a correction term for the Gibbs free energy change of formation (ΔG_f) of each oxide. This correction term is determined by calculating the difference between the Gibbs free energy change of formation of the silicate minerals and the sum of the free energies of their constituent oxides. This difference is the formational free energy for the compound and is shared between the oxides to give the *effective* Gibbs free energy change of formation ($\Delta G_f'$). In this study a set of likely minerals is calculated from the weight percent of oxides in the parent rock and these are then used to find the correction factor. In order to determine the mineral assemblage of a rock from bulk chemical analysis a mineral norm is calculated. The norm is a set of *idealised* minerals that are calculated from the known composition of oxides in a rock. The method of calculating the minerals likely present is detailed in the Appendix.

2.1.2 Percolation and leaching

Percolation

The rate of water flowing through each soil layer is regulated by the amount of pore space available in that layer. In the early stages of soil formation this is dependent only

upon the porosity of the bedrock, however, over time, the losses due to leaching increase this porosity. The pore space is expressed as a fraction of soil volume ($m^3 m^{-3}$) and is derived from the proportion p of original parent material remaining in the profile, where $p = 1$ for unweathered bedrock and $p = 0$ for complete loss of the original material. The total soil deficit w below depth z is calculated as

$$w(z) = \int_{\infty}^{z} (1 - p) \mathrm{d}z \quad (2)$$

and has the dimension of length. The coordinate system is chosen such that z is positive in the downward direction.

A simple vertical flow through the profile is assumed, with sub-surface flow resulting from the vertical variation in pore space. The percolation of water, F, at depth z is

$$F(z) - F_0 = K w(z) \quad (3)$$

where F_0 is the rate of percolation allowed through the bedrock and K is a site specific parameter related to hydraulic conductivity and slope gradient. Because $F(z)$ is the maximum rate of percolation, effectively occuring percolation is whichever is lowest, the maximum rate of percolation or the rate of precipitation minus the cumulative evaptranspiration from the soil surface to depth z.

Evapotranspiration

The process of evapotranspiration removes water from the soil profile. Here we calculate total actual evapotranspiration (E_T) as the minimum of potential evapotranspiration (E_T^*) and mean annual precipitation (P_A):

$$E_T = \min[E_T^*, P_A]. \quad (4)$$

Although simple, the formulation still permits the model to operate under water stressed conditions. E_T^* is calculated for specific locations using a modified Hargreaves

model (Hargreaves and Samani, 1985) (see Appendix). This method is chosen because it requires only a small amount of climate data (temperature) for any specific location. The allocation of water loss by evapotranspiration to the different soil layers is determined by the distribution of roots through the soil profile, these are assumed to decline exponentially with increasing soil depth (Jackson et al., 1996). The e-folding rooting scale depth is z_r so that the rate of evapotranspiration, E, at depth z is

$$E(z) = \frac{E_T}{z_r} \exp^{\frac{-z}{z_r}}. \quad (5)$$

Rainfall minus cumulative evapotranspiration at depth z places a limit on the amount of water available for percolation:

$$E_c(z) = E_T(1 - \exp^{\frac{-z}{z_r}}) \quad (6)$$

where $E_c(z)$ is the cumulative evapotranspiration from the surface down to depth z. Values for z_r can be obtained from the rooting distributions compiled for different biomes by Jackson et al. (1996). When the modelled soil is shallow, the rooting depth and subsequent vertical distribution of evapotranspiration is limited by the soil depth. Rooting depth, d_r, is the depth which contains a fraction, f, of the total root mass (Arora and Boer, 2003) and can be calculated by

$$d_r = -\ln(1 - f)z_r. \quad (7)$$

If we term rooting depth as the depth above which 95 % of the total root biomass is contained, following Arora and Boer (2003) we use $f = 0.9502$ to aid simplicity, so that

$$d_r = -\ln(1 - 0.9502)z_r = 3z_r \quad (8)$$

When d_r is greater than the soil depth in either the early stages of soil development or in shallow soils, the above value of z_r is adjusted so that d_r equals soil depth. This will result in a greater proportion of roots in the top layers of soil.

Leaching

Loss of solutes from the profile can be calculated by mass balance (Fig. 1). The amount of solute carried into a soil volume at depth z by percolating water is $F(z)c_i$, where c_i ($g\,m^{-3}$) is the concentration of ion i in solution. The amount of solute lost from the volume element by diversion due to sub-surface flow is $\delta F(z)c_i$ and due to percolation outflow $(F(z) + \delta F(z))(c_i + \delta c_i)$, thus

$$-\delta m_i \delta z = [-(\delta F)c_i - Fc_i + (F + \delta F)(c_i + \delta c_i)]\delta t \quad (9)$$

where m_i is the mass change of oxide i at depth z during time δ_t. Neglecting second order terms this reduces to

$$\frac{\partial m_i}{\partial t} = -F(z)\frac{\partial c_i}{\partial z}. \quad (10)$$

The proportion, p_i, of oxide i remaining is then calculated from the original bedrock density and the loss of mass from leaching

$$p_i^{t+1} = p_i^t - \frac{m_i}{m_i(t = 0)} \quad (11)$$

where $m_i(t = 0)$ is the mass of element i in the original parent material ($\rho_{bedrock}$ × wt% of i).

2.2 Ionic diffusion

The ions released into solution from weathering can diffuse from regions of higher to lower concentrations according to

$$\frac{\partial c_i}{\partial t} = \frac{\partial}{\partial z}\left(D_l(z)\frac{\partial c_i}{\partial z}\right) \quad (12)$$

where D_l is the diffusion coefficient of the ions which for current purposes we keep fixed for all elements. This process is most important at the weathering front where ion concentrations are greatest and leaching losses are low (Kirkby, 1985).

2.3 Bioturbation

Bioturbation is the mixing and turnover of soil resulting from biological activity and is considered a major soil forming process (Gabet et al., 2003; Wilkinson and Humphreys, 2005; Yoo et al., 2005). Bioturbation is represented in the model as a diffusive process:

$$\frac{\partial p_i}{\partial t} = \frac{\partial}{\partial z}\left(D(z)\frac{\partial p_i}{\partial z}\right) \tag{13}$$

where p_i is the proportion of element i remaining in the profile at depth z and D ($m^2\,yr^{-1}$) is the diffusion coefficient. It is assumed that the mixing intensity will decline with depth due to the decrease in faunal activity with increasing soil depth (Humphreys and Field, 1998; Wilkinson and Humphreys, 2005; Johnson et al., 2014). In the model this takes the form of an exponential relationship:

$$D(z) = D(0)\exp^{-z/z_b} \tag{14}$$

where $D(0)$ is the diffusion coefficient at the soil surface and z_b is the e-folding length scale for biological activity (m). The boundary conditions at the top and bottom of the profile allow no mixing in or out so that

$$\frac{\partial p_i}{\partial z} = 0 \tag{15}$$

at $z = 0$ and $z = Nz$, where Nz is the total number of vertical layers in the model.

2.4 Surface erosion

Removal of soil from the surface by mechanical processes is modelled through a denudation rate, T ($m\,yr^{-1}$). Surface elevation, z_s is lowered at a rate, dz_s/dt, which is inversely proportional to the amount of original material remaining at the surface, p_s,

or $p(z = 1)$. In the model this lowering process shifts soil properties (or proportion of substance remaining, p) up the soil profile and thus

$$p(z - \delta z, t + \delta t) = p(z, t) \tag{16}$$

and

$$\frac{\partial p}{\partial z}(-\delta z) + \frac{\partial p}{\partial t}\delta t = 0 \tag{17}$$

or finally

$$\frac{\partial p}{\partial t} = \frac{\partial p}{\partial z}\frac{\delta z}{\delta t} = \frac{\partial p}{\partial z}\frac{T}{p_s}. \tag{18}$$

Cosmogenic nuclides such as in-situ ^{10}Be have provided measures of surface erosion for hillslope soils where soil thickness is assumed to be at steady-state and thus rates of soil production from bedrock balance rates of loss due to surface erosion. Erosion rates calculated from these studies lie in the range of 10 to 100 $m\,M\,yr^{-1}$ (Wilkinson and Humphreys, 2005).

2.5 Organic carbon and CO_2

2.5.1 Carbon fluxes, decomposition and mixing

To estimate carbon input into the soil we assume that vegetation cover is at steady-state, with new carbon production equal to the losses from litterfall and root senescence. For this first presentation and evaluation of the model we simply assume a time invariant climate and annual net productivity (N_P) ($kg\,C\,m^{-2}\,yr^{-1}$). The carbon is assigned to four different pools which are defined by the stability or turnover time of the pools. These are fine litter (e.g. leaves), coarse woody debris (e.g. branches/stems),

fine roots and coarse roots. The overall equation for the organic matter decomposition and mixing processes in the soil profile is

$$\frac{\partial C_i}{\partial t} = \frac{\partial}{\partial z}\left(D(z)\frac{\partial C_i}{\partial z}\right) - k_i(z)C_i + I_i(z) \tag{19}$$

where C_i is the concentration of carbon (kg m^{-3}) in pool i, the first term is the diffusive mixing of carbon through the soil profile by biological activity, k is the decay coefficient (yr^{-1}) and I_i is the carbon entering the soil profile from either plant litter at the surface or from root litter which is distributed throughout the profile. The decay coefficient may remain constant with depth or decrease with increasing soil depth as observed in soil carbon studies using carbon isotopes (Veldkamp, 1994; Trumbore et al., 1995; Van Dam et al., 1997). For this study it is assumed that the decay rate, k, declines exponentially with increasing soil depth. For the fine and coarse litter, I provides a top boundary condition flux equal to $\alpha_i N_P$ where α_i is the proportion of carbon production assigned to pool i. For both fine and coarse roots the input of carbon is distributed vertically throughout the profile according to

$$I(z) = \frac{\alpha_i N_P}{z_r} \exp^{\frac{-z}{z_r}}. \tag{20}$$

Because of the much shorter timescale that these carbon dynamics operate on, we assume a steady-state carbon profile and hence solve Eq. (19) for $\partial C/\partial t = 0$ and boundary conditions of $\frac{\partial C}{\partial z} = 0$ at the bottom and a top boundary condition equal to the flux of carbon entering from the above litter. The carbon is not subject to the modelled surface erosion, however, given the very different timescales of the two processes this seems a reasonable simplification. A limitation of this carbon scheme is that biomass is present from the start of soil evolution rather than vegetation productivity evolving with the developing soil profile. This may result in an unrealistic vegetation enhanced acceleration of weathering in the very earliest stages of soil evolution.

2.5.2 CO_2 production and diffusion

Gases in soil are transported in either the pore space or in solution. Here we assume that the CO_2 produced from root respiration and from the above decomposition process is transported through the profile by gaseous diffusion only. This is modelled as a diffusion scheme:

$$\frac{\partial C_g}{\partial t} = \frac{\partial}{\partial z}\left(D_c(z)\frac{\partial C_g}{\partial z}\right) + S(z) + R_c(z) \tag{21}$$

where C_g is the concentration of CO_2 (kg m^{-3} soil air), D_c(z) is the diffusion coefficient of CO_2 in soil (m^2 s^{-1}) at depth z, S is the CO_2 production rate (kg m^{-3} s^{-1}) (calculated by $\sum_{i=1}^{n} k_i(z)C_i(z)$, where n is the total number of carbon pools (4 in this case)) and R_c is the production of CO_2 from root respiration which is assigned from the literature and distributed throughout the profile following the same exponential function as for root carbon turnover. The effective diffusion coefficient in soil air is lower than that for bulk air due to both the smaller volumes of air filled pore space and the tortuosity introduced by soil pores. The diffusion coefficient for CO_2 is taken from Jones (1992), $D_c = 14.7$ (mm^2 s^{-1}) for 20 °C. To account for tortuosity a more realistic diffusion coefficient for soil air (D_s) is calculated using the following relationship of Penman (1940) (Hillel, 2004, pg. 204).

$$\frac{D_s(z)}{D_c} = 0.66 f_a(z) \tag{22}$$

where f_a is the fraction of air-filled space, in the model this is equal to $1 - p(z)$. 0.66 represents the tortuosity coefficient, which means that the straight line path is approximately two-thirds the length of the path of diffusion, so as the pore space increases the

diffusive path will decrease. The CO_2 profile is also modelled at steady-state so that

$$\frac{\partial C_g}{\partial t} = 0 \tag{23}$$

The top boundary condition is equal to the atmospheric concentration of CO_2 and the bottom boundary condition allows no mixing out of the profile. This modelled partial pressure of CO_2 replaces the atmospheric CO_2 concentration used in the carbonate equations of the dissolution model and thus changes the charge balance of Eq. (1), influencing the pH of the soil solution and solubilities of the rock oxides.

2.6 Nutrient cycling

Nutrient concentrations in vegetation depend on a number of factors such as the species of plant, the climate and the nutrient status of the soil. As a simplification, it is assumed in the model that the nutrients taken up and those re-entering the soil from plant litter and root turnover have fixed stoichiometric ratios. McGroddy et al. (2004) have found that within forest biomes, foliar C : N : P ratios are reasonably well constrained, with C : N ratios in litter globally similar.

We use the optimum stoichiometric nutrients ratios calculated by Linder (1995) for deciduous plants. For the following elements N : P : K : Ca : Mg : Fe these are 100 : 10 : 35 : 2.5 : 4 : 0.2. Nutrient concentrations are calculated assuming a fixed proportion of biomass is made up of nutrients and a fixed relationship between N_P and biomass production (biomass is double the mass of carbon). The nutrients are released into solution at the soil surface ($g m^{-2} yr^{-1}$) from the fine litter pool and provide a flux surface boundary condition in the solute transport equation (Eq. 10). The nutrients from fine root turnover are released into solution obeying the exponential decline in root distribution with depth. Although obviously not completely realistic, it has been observed that nutrients are readily lost from litter in the earlier stages of decomposition (Berg and McClaugherty, 2008) and this method makes it possible to readily incorporate the nutrients into the dissolution submodel.

Nutrients are then taken up from solution by the vegetation or leached from the system. Nutrient uptake from the soil profile is passive and controlled by the rate of evapotranspiration from each soil layer, the concentration of ions in solution in that layer and the rate of uptake required by the vegetation i.e. the fraction of biomass production calculated from N_P. This process is represented by the second term in an updated form of Eq. (10):

$$\frac{\partial m_i}{\partial t} = -F(z)\frac{\partial c_i}{\partial z} - \frac{\partial E_c}{\partial z} c_{ni}(z) + R_{ni}(z). \tag{24}$$

where c_n is the concentration of nutrient i in each layer ($g m^{-3}$). Total c_{ni} is calculated by integrating $\frac{\partial E_c}{\partial z} c_{ni}$ successively over each soil layer until the required annual uptake of nutrients is reached (i.e. when total uptake of nutrient i equals the nutrient production calculated from biomass production and hence turnover for the steady-state condition). R_{ni} is the concentration of nutrient i returned from fine root turnover ($g m^{-3} yr^{-1}$). When the nutrient uptake from a layer is greater than $c_n \times \Delta t$, uptake is set to $c_n / \Delta t$. We know that plants can interact directly with soil minerals for nutrients, however, the main source of nutrients is likely the soil solution (Lucas, 2001) and this simple mechanism of nutrient uptake is employed for the first attempt at modelling long-term, plant-soil interactions.

3 Model solution and parameters

The model partial differential equations are solved numerically by finite-difference schemes. The leaching and denudation equations are solved by an upwind scheme (Morton and Mayers, 2005) and the diffusion equations by the semi-implicit Crank-Nicholson scheme (Morton and Mayers, 2005). The parameters used in the model runs in the following section are shown in Table 1. The values are selected as being the most appropriate from the literature, they are not constrained for one particular site.

4 Model behaviour

In this section to permit easier interpretation of our model predictions we follow a hierarchial procedure. This involves first running the model in it's most basic form and adding an additional process for each subsequent run. We can then get a clear sense of how each of the important processes influences the modelled soil properties and thus understand their importance in soil evolution within this modelling framework.

In the following simulations the oxide composition of the model bedrock is a basalt taken from the study of a Hawaiian soil chronosequence (Porder and Chadwick, 2009) (Table 2, Kona flow). For the purpose of this study the model is run first with only oxide weathering and leaching as the active processes. Other processes are then added successively in the order of surface erosion, bioturbation, organic carbon decomposition and nutrient cycling. For the simulations that follow, the profile is discretised into 10 cm deep layers and the total number of layers is chosen so that the total profile depth is greater than that reached by the weathering front during the simulation. The model timestep is 0.1 year. Unless stated otherwise the model is run with the parameters in Table 1, and a mean annual temperature and precipitation of 20 °C and 1.7 m yr^{-1} respectively.

The developmental state of the modelled soil profile is quantified as the proportion of each oxide remaining in the soil layers relative to that of the parent material. Values lower than one represent a relative loss from the profile compared to the inital unaltered bedrock material and values greater than one relative enrichment. A value equal to one indicates zero mobility.

4.1 Dissolution and leaching

With chemical weathering and leaching as the only active processes, we observe losses of the most souble oxides in only the top 20 cm of the soil profile (Fig. 2, first column). The sequence of losses for the basic oxides is $MgO > Na_2O > CaO \gg K_2O$ (Fig. 4) after 20 thousand years of soil development. Of the non-basic oxides, we ob-

serve some depletion of P_2O_5 and SiO_2 but very minimal losses of FeO and Al_2O_3 (Fig. 3, first column and Fig. 4). The solubility of iron increases at lower pH values and Fig. 4 demonstrates the much greater losses of Fe when all processes are included in the model simulation and soil pH has lowered from approximately 8 to 6. Al_2O_3 on the other hand displays reduced losses in the full simulation and this is attributed to aluminium being most soluble in either very alkaline or acidic solutions. At this stage the model displays very early signs of horizonisation, with a depleted top (or A) horizon and a slightly enriched saprolite (or B) horizon. Enrichment or deposition of the most soluble oxides at the bottom of the weathering front occurs when saturated solution from the layers above percolates into a bedrock layer with lower equilibrium solute concentrations. At this most elementary stage of the model the weathering sequence of basic oxides displays similar weathering sequences to other studies. For example Busacca and Singer (1989) observe a mobility sequence of $Mg \gg Na > Ca > K$ from alluvium deposits in California and White et al. (2008) observe a weathering sequence of $Mg > Ca > Na > K$ in marine terraces also in California. For the three basic oxides found in the feldspar family of minerals, CaO, Na_2O and K_2O, the modelled sequence of losses follow an expected trend associated with the lower solubility of K-feldspar (or orthoclase) compared to plagioclase which incorporates the endmembers anorthite and albite (Nesbitt and Young, 1984; White et al., 2001, 2008). Importantly, White et al. (2008) calculate that the pore waters of their chronosequence rapidly reach feldspar thermodynamic saturation and so the weathering velocity of Ca, Na and K is controlled by this thermodynamic state, the rate of which is determined by the flux of water, this being the weathering mechanism of this model. White et al. (2008) also found that the weathering of plagioclase is non-stoichiometric, i.e. there is selective removal of Ca over Na from plagioclase in their marine terraces. Thus the solubility of the oxides act independently, indicating that so far the dissolution and leaching of mineral oxides in this model is conceptually realistic.

Even though the current model does not predict secondary mineral formation, it is still possible to predict the secondary minerals likely to be present through an under-

standing of the sequence of minerals formed across gradients of weathering intensities. The modelled weathering sequence thus predicts the commonly predicted weathering pathway of a shift from predominantly silicate minerals such as the Mg, Ca and K feldspar family to the secondary Fe and Si containing clays such as vermiculite and montmorillonite, through to the Al and Si containing clay mineral kaolinite present in weathered soils. Eventually, in very weathered soils Al sesquioxides such as gibbsite dominate (Tardy et al., 1973).

The predictions based on chemical weathering and leaching processes alone demonstrate (i) an expected weathering sequence of oxide losses, (ii) an increase in the depth of the weathering front with increasing time since the intiation of soil development, (iii) very shallow soil profiles in the absence of any physical weathering or biological activity and (iv) evidence of horizonization.

4.2 Surface erosion

The modelled process of surface erosion acts by shifting the simulated soil properties towards the soil surface, whilst removing those in the surface layers (Figs. 2 and 3, second column and Fig. 5). Erosion plays a larger role in older, more depleted soils. This is demonstrated when all processes are included in the model simulations (Fig. 5). The more weathered and depleted in original material the surface layer is, the greater the reduction in surface elevation, with a shallower profile then ensuing. Thus over long timescales surface erosion becomes an increasingly important process in the soil evolution model. If the rate of soil deepening becomes equivalent to the rate of surface denudation, soil thickness naturally reaches a steady-state.

4.3 Bioturbation

Parameterised here as a diffusion process, bioturbation smoothes the oxide distributions in the surface layers (Figs. 2 and 3, third column) allowing the upward mixing of oxides from further down the profile. This action combined with that of surface erosion

results in retention of mineral oxides in the surface layers (Fig. 4). Bioturbation acts to deepen the soil by removing material from deeper in the profile and mixing it into the upper layers. Bioturbation thus influences both the composition of the soil layers and the rate of soil production from bedrock.

4.4 Vegetation interactions

The modelled vegetation interacts with the soil via three processes: by the uptake of water from the soil, by increasing soil acidity through the production of CO_2 from root respiration and litter decomposition, and through the cycling and retention of nutrients. Vegetation thus potentially plays an important role in modelled soil development.

At steady-state the highest carbon stocks are in the surface layers (Fig. 6). For the control run when the rate of decomposition, k, declines with increasing soil depth, the carbon persists in the deeper soil layers (1–2 m) (Fig. 6a), whereas, when the decay rate of the carbon pools remains constant with depth, organic carbon is absent below 1 m (Fig. 6b). The comparisons with observed below-ground carbon concentrations suggest that the decreasing decay rate with increasing soil depth is perhaps the most realistic formulation (Fig. 6).

The addition of organic matter to the soil accelerates the weathering of all but the most insoluble oxides (Figs. 2 and 3, column 4). When carbon biomass is absent from the model simulation, soil development progresses slowly, CO_2 concentrations are equal to atmospheric concentrations, and pH remains above 7. When organic carbon is included in the model simulations pH decreases from ~ 8 in the surface layers to ~ 6 after 20 thousand years of soil development (Fig. 2, column 4 and Fig. 4).

This decrease in pH and increase in leaching losses is a result of the higher concentrations of soil CO_2 (Fig. 7). CO_2 concentrations increase with increasing soil depth, reaching over 100 times atmospheric levels in the early stages of soil development when pore space is low (Fig. 8). The CO_2 concentrations in the soil profile decrease over time from very high initial concentrations due to the creation of pore spaces in the soil profile which allow the CO_2 to diffuse to areas of lower concentrations. Soil CO_2

concentrations are highest when the carbon productivity is highest (Fig. 8) because of the greater inputs of organic carbon into the soil. Deeper root profiles result in higher soil CO_2 concentrations at deep depths (Fig. 8c). This is due to the higher inputs from root decomposition and root turnover at these depths and lower tortuosity which hinders CO_2 diffusion into and out of the surface layers. For this simulation the flux of CO_2 out of the soil profile is within the ranges observed in studies of Hawaiian tropical forest soils (Fig. 9).

The addition of nutrient cycling into the simulation results in some retention of the oxides in the surface layers (Figs. 2 and 3, column 5), a trend also noted in the soil-nutrient studies of Jobbágy and Jackson (2001); Lucas (2001) and Porder and Chadwick (2009). However, in older or very wet soils the effect of plants on nutrient retention may be diminshed due to the overriding effect of leaching losses as found by Porder and Chadwick (2009). In the model the return of basic ions in solution from litter decomposition alters the equilibrium status of the solution and slows the rate of dissolution.

This step-wise approach of including processes in the model framework has demonstrated the important role vegetation plays throughout modelled pedogenesis and thus highlights the possible significant influence that vegetation may have on the long-term carbon cycle and hence climate.

5 Comparison of model predictions with observations

To assess the ability of the model to reproduce real soil profiles we compare the model predictions with data from in-situ soil profiles from soil chronosequences. Due to the slow nature of pedogenesis it is impossible to directly observe soil changes over these very long timescales. Instead we make use of chronosequences. These are series of soils which differ in the age of soil initiation but other factors of soil formation such as parent material, climate and topography remain constant. It is thus assumed that any differences in soil properties are related only to the differences in the age of the soil profile.

Hawaiian soil chronsequence data published by Porder et al. (2007) and Porder and Chadwick (2009), are used for comparison here. The soils have developed on volcanic lava flows on the island of Hawaii, and thus have a parent material of relatively uniform composition (Table 2). Because of the wide range in eruption ages, soils from the Hawaiian island chain have been utilised in a number of studies looking at the interactions between soil age, weathering and nutrients (Vitousek et al., 1994; Vitousek and Farrington, 1997; Chadwick et al., 1999; Hedin et al., 2003; Porder et al., 2007; Porder and Chadwick, 2009). Porder et al. (2007) sampled soils on three lava flows aged 10 ka, 170 ka and 350 ka, each spanning a topographic gradient and resulting rainfall gradient. Mean annual precipitation (P_A) varies from 0.57 m yr^{-1} to 2.5 m yr^{-1}, the highest rates of precipitation are found at the highest elevations. Mean annual temperature (T_A) increases from 16 °C at these higher and wetter elevations to 24 °C at the lower altitudes. Consequently the sites receiving the lowest rainfall have the highest temperatures and are thus subject to the highest E_T, resulting in a negative water balance (Chadwick et al., 2003). It is important to note that the rainfall gradient has not always been this strong during the evolution of the soil profiles, this is a result of glacial periods and changes in the elevation of the trade wind inversion (Hotchkiss et al., 2000). The sites at the wet, higher elevations may have received 50 % less precipitation during most of their development, however, the temperatures during these drier glacial periods were also cooler, thus probably reducing the water lost from the profile by evapotranspiration.

The model is compared with the driest and wettest sites from each flow and an intermediate rainfall site. The following model parameters are modified from those in Table 1 to suit the Hawaiian sites. The monthly minimum and maximum and mean temperatures needed to calculate E_T using the Hargreaves equation are taken from the Western Regional Climate Center (http://www.wrcc.dri.edu/). The site closest to the Kona lava flows is used and the temperatures were adjusted to T_A of 16 °C, 20 °C and 24 °C for the low, medium and wet rainfall sites respectively. The estimated E_T^* calculated for these sites is 1.20, 1.34 and 1.48 m yr^{-1} respectively. We assign productivity

values for each site by relating E_T to productivity using a water use efficiency (WUE) term. The WUE of a plant is the unit of carbon fixed per unit of water transpired. Assigning a WUE of $1\,kg\,m^{-3}$ we estimate carbon productivity (N_P) values of 0.3, 0.53 and $0.48\,kg\,m^{-2}\,yr^{-1}$ for each of the sites respectively, replicating the observed trend for Hawaiian vegetation of increasing N_P with P_A up to approximately $2\,m\,yr^{-1}$, decling for further increaes in rainfall (Schuur and Matson, 2001; Austin, 2002). However, we are aware that the mechanisms behind this relationship are not the same. The decrease in the model productivity is due to decreasing evapotranspiration associated with decreasing P_A, whereas, the changes in the observations are thought to be due to decreased N availability. The vertical root depth scale (z_r) is 0.26 m, the value estimated for tropical evergreen forests (Jackson et al., 1996). The bedrock oxide compositions used in the model runs are shown in Table 2. The erosion rate is set to $10\,m\,Myr^{-1}$ because even though the soils sampled are not thought to have experienced high rates of erosion (Porder et al., 2007), even stable soils often experience erosion rates greater than $5\,m\,Myr^{-1}$ (von Blackenburg, 2005) and values in the range of 7.7 to 12 m Myr^{-1} were calculated for basalts on the lip of Hawaiian volcano craters (Craig and Poreda, 1986; Kurz, 1986; Nishiizumi et al., 1990). Townsend et al. (1995) found that the turnover times of the intermediate carbon pool in Hawaii soils double with a 10 °C decrease in T_A. It is unclear whether this increase in decomposition with increasing temperature follows a linear or exponential trend but here we assume a simple linear function of decomposition with mean annual temperature using the values observed by Townsend et al. (1995) to calculate the decomposition rate (k) of the coarse roots and coarse wood:

$$k_{coarse} = 0.0026.T_A - 0.02 \quad (25)$$

The decomposition rates (k) of the fast carbon pools remain the same as in Table 1. The depth of the vertical model layers is increased to 0.25 m to improve the numerical stability of the simulations.

To determine the intensity of weathering of elements in a soil profile, element concentrations are commonly compared with those in unweathered bedrock and normalised to an immobile element such as zirconium (Zr) to give the fraction of the particular element remaining relative to bedrock (Brimhall and Dietrich, 1987) (See the Appendix for a description of this method). For these Hawaiian soils Porder et al. (2007) used Niobium (Nb) as the immobile element. This provides values which can be directly compared with output from the model.

It is recognised that soils are complex systems and display a great deal of heterogeneity across even very small spatial scales. Nevertheless, we assume here that over these pedogenic timescales the soils sampled at each of these sites have been subject to the same soil-vegetation interactions.

Figure 10 illustrates the performance of the model for the three different rates of annual precipitation on the young 10 ka lava flow for a selection of elements. The simulations of Ca and Na in the model are most realistic, followed by Mg, and then K and P. The model captures the slower rate of weathering losses in the driest site and higher rates in the intermediate and high rainfall sites. Mg, Ca and Na display very similar distributions of depletion in these Hawaiin soils, whereas the relative vertical distribution of Mg depletion differs from that of Ca and Na in the model. Modelled Mg weathers to deeper depths than those observed in the intermediate rainfall sites (where model N_P is highest), also weathering deeper than the other model elements. Modelled K is particularly resistant to weathering compared with the observations. K is required by plants in larger amounts than Ca and Mg and is thus strongly cycled (Jobbágy and Jackson, 2001). The model results for K may thus highlight the importance of the active role of plants, mycorrhiza and faunal communities in mediating the release of this poorly mobile nutrient from minerals (Hutchens, 2009). The uptake of nutrients in the model is controlled by the rate of evapotranspiration and concentrations of the nutrient in the soil solution, however, there are a number of other mechanisms by which plants can aquire nutrients (Hinsinger et al., 2009). For example, roots can actively induce the release of non-exchangeable K from phyllosilicates by secreting H^+ to exchange with K. By

actively taking up K from solution plants can also shift the solution equilibrium thus promoting further dissolution (Hinsinger et al., 1993; Hinsinger and Jaillard, 1993). By altering the solubility of K in our model, we show that the missing process accelerates the weathering of K from minerals by a factor of approximately 50 (Fig. 11). Modelled P is even more immobile than K, however, the observations also exhibit little depletion of P in these young profiles. The 10 ka flow is characterized by surface layers enriched in P and low amounts of P depletion in the deeper layers of the intermediate and wet sites. For the driest site (Porder and Chadwick, 2009) argue that the soils must receive additional P from exogenous sources. If this enrichment was due to cycling of the nutrient we would expect this surface enrichment to be balanced by depletion deeper in the profile, which is not observed. Dust can be a significant source of P to Hawaiin soils (Chadwick et al., 1999), but for these young flows Porder and Chadwick (2009) suggest that the addition of fine organic matter from nearby surroundings may explain the additions. Without these external sources of P, the relative immobility of modelled P may be representative of these young soils.

For the 170 ka Hawi flow, both the Hawaiian and modelled soils have weathered much deeper in the intermediate and high rainfal sites compared with the younger 10 ka flow. The model captures the lower losses in the dry site relative to the wetter sites but does not replicate the more enriched surface layers (Fig. 12). The modelled Na and Ca profiles again match the observations most closely, reproducing the nearly totally depleted profiles at the wetter sites and even matching the depth of weathering. The depth of the Mg weathering front, however, is still too deep and the modelled K and P profiles indicate that the modelled processes are still too resistent to weathering for these elements. It should be noted that Porder et al. (2007) estimate that additions of dust to the Hawi flow averages 30 % of the total mass lost from the profiles and most of this dust is found in the top 30 cm which may obscure some of the weathering signal in these soils.

The 350 ka Pololu flow differs from the 10 ka and 170 ka flow by being underlain by a pahoehoe flow at 1.8 m. Pahoehoe flows are characterized by smooth, glassy sur-

faces and are less porous than the overlying, blocky lava flows. They therefore act as a barrier to weathering in these soils. By comparing the profiles of K with Na Porder and Chadwick (2009) show that even at this age, plants in the dry flow are still enriching the surface layers with nutrients but in the intermediate and high rainfall sites, leaching losses override any nutrient retention and the surface layers are depleted in nutrients. Figure 13 shows that for the dry site the model displays general agreement with weathering depths and again Na shows the closest match to the observations followed by Ca and Mg with K and P still too immobile at this age. The slow rate of chemical weathering of these two elements in the model also means that any depleted signal in the surface layers will also be removed by surface erosion. For the intermediate and wet rainfall sites the model captures the surface losses of Na, Ca and Mg, K is still is still too resistant in the intermediate site but agrees better at the wettest site. For this older soil, modelled P shows some signs of depletion but is still much more resistant than the observed profiles. In the Hawaiian soils P losses are correlated with Fe losses in the old and wet sites, Fe can bind with P and may drive the losses in these lower oxygen, reducing soils (Porder and Chadwick, 2009), a process not represented in the model. The modelled profiles extend to nearly five metres for the two wetter sites whereas the observed profiles reach a maximum of 1.8 m because of the impermeable pahoehoe layer at this depth.

Figure 14 shows the comparisons between the observations and modelled pH profiles. Modelled pH agrees best with observations in the driest sites and for the intermediate aged, Hawi flow. Simulated pH is generally too high in the wetter sites which could be because modelled Al_2O_3 is very insoluble (Fig. 3) so Al^{3+} ions in solution may be lower.

These comparisons show that for all profiles modelled plant nutrients P and K are not in agreement with the observations. That Na, which is not an essential plant nutrient, shows the best match, followed by Ca, which is a plant nutrient but is thought to be taken up in amounts equivalent to availability and depends on water flow to the vegetation (Knecht and Goransson, 2004), suggests that it is the process of nutrient

uptake which the model is not reproducing realistically. The good agreement with Na, particulary in the intermediate rainfall sites where plants play an important role in nutrient distributions suggests a good model understanding of the other soil processes included in the model and thus that the model will provide a reliable platform for further developing our understanding of nutrient dynamics.

6 Conclusions

This study has demonstrated that the soil evolution model presented is capable of reproducing realistic soil properties such as relative elemental losses, weathering depths, pH profiles, organic carbon content and soil-pore CO_2 concentrations. The model requires 20 parameters, of which at least 13 are easily assigned from literature, plus regional climate, bedrock data and simple thermodynamic constants to simulate soil genesis on a chosen parent material. The limited number of processes and the ease at which they can be both included and excluded from simulations makes the model behaviour easy to understand. This study has detailed how each of these model processes interacts with and influences the soil properties.

Comparisons of the model predictions with a Hawaiian soil chronosequences has highlighted the importance of vegetation in shaping soil profile evolution by increasing soil acidity and cycling nutrients. The good model agreement with the observations of Na, Mg and Ca which are less strongly cycled by vegetation, suggests that the model is realistically reproducing the other processes unrelated to nutrient cycling. These results lend confidence to the model's ability to quantify processes and feedbacks occuring during pedogenesis and to the valuable role it can play in understanding long-term biogeochemical cycles.

Minasny et al. (2008) highlight a number of criteria that a pedogenetic model should comply with, these are (1) the model should be based on physical laws (2) the model should be able to simulate the present condition given the initial condition, particularly soil thickness and soil property variation in the landscape (3) the model should be

able to simulate the likely past condition or trend in the condition given the current condition and (4) the model should create soil horizons. The adapted Kirkby (1985) model presented here shows promise for each of these criteria and the similarities between the model and the observed soil profiles demonstrates the model potential for soil evolution studies and for understanding feedbacks between the soil and biosphere.

It is, of course, acknowledged that there are many important pedogenic processes missing from the model. For example: (i) the model does not predict secondary mineral formation or size fractions so features such as cation adsorption and soil structure associated with these properties are overlooked, (ii) porosity is very simple, and pores are assumed to be free draining and connected, which for tropical soils may be acceptable (Sander, 2002) (iii) the formulation of hydraulic processes is very simple and should ideally be better constrained, (iv) organic matter only interacts with the soil through the action of increasing acidity so again missing out associated cation exchange and structural properties and (v) at the moment plant productivity does not evolve with nutrient availability. However, many of these missing processes can be included in the model framework with relative ease once the method and relevant parameters are derived. For example, to best predict secondary mineral mineralogy the model could in future utilize a more complex chemical reaction module, for example by coupling with the PHREEQC geochemical programme (Parkhurst and Appelo, 1999).

Appendix A

A1 Dissolution reactions

The Law of mass action states that the rate of a reaction is proportional to the product of the active masses of reactants and at equilibrium the rate of the forward reaction is

equal to the rate of the backward reaction:

$$bB + cC \rightleftharpoons dD + eE \tag{A1}$$

Equation (A1) represents the reaction between b moles of B with c moles of C in equilibrium with d moles of D and e moles of E. The equilibrium constant K of the reaction is related to the above by

$$K = \frac{aD^d aE^e}{aB^b aC^c} \tag{A2}$$

where a is the *activity* of each reactant and product. This thermodynamic equilibrium constant is related to the Gibbs free energy of the reaction (ΔG_r) by

$$\Delta G_r = -RT \ln K \tag{A3}$$

where R is the universal gas constant ($\mathrm{J\,mol^{-1}\,K^{-1}}$), T is temperature (K) and

$$\Delta G_r = \Sigma \Delta G_{f\ \mathrm{products}} - \Sigma \Delta G_{f\ \mathrm{reactants}} \tag{A4}$$

where ΔG_f is the Gibbs free energy change of formation, which is the change in Gibbs free energy that accompanies the formation of 1 mol of a substance in its standard state from its constituent elements in their standard states. To calculate the equilibrium composition at temperatures other than 20 °C, the Gibbs-Helmholtz equation can be used.

The following is an example of the simplified dissolution reaction for SiO_2 in water and the procedure of how this is calculated in the model:

$$SiO_2 + 2H_2O \leftrightharpoons H_4SiO_4 \qquad \Delta G_r = 5.47 \tag{A5}$$

$$SiO_2 + 2H_2O \leftrightharpoons H_3SiO_4^- + H^+ \qquad \Delta G_r = 18.71 \tag{A6}$$

$\Delta G_r = -1.364 \log K$ therefore

$$-\frac{5.47}{1.364} = \log \frac{[H_4SiO_4]}{[SiO_2][H_2O]^2}. \tag{A7}$$

The activity of H_2O is unity so

$$-4.01 = \log[H_4SiO_4] - \log[SiO_2] \tag{A8}$$

$$[H_4SiO_4] = [SiO_2] \times 10^{-4.01} \tag{A9}$$

and for $[H_3SiO_4]$ the equivalent equation is reduced to

$$[H_3SiO_4^-] = \frac{[SiO_2] \times 10^{-13.72}}{[H^+]} \tag{A10}$$

Similar reactions occur for the other oxides present in the parent material. Table A1 shows the Gibbs free energy of formation for the oxides used in the model reactions. The concentration of H^+ in the modelled soil solution is calculated by balancing the anions and cations in solution. The relevant mass balance equation is

$$[H^+] + [Al(OH)_2^+] + 3[Al^{3+}] + [Na^+] + [K^+] + 2[Ca^{2+}] + 2[Mg^{2+}] + 3[Fe^{3+}] + 2[Fe^{2+}]$$
$$= [HCO_3^-] + [OH^-] + 2[CO_3^{2-}] + [Al(OH)_4^-] + [H_3SiO_4^-] + 2[HPO_4^{2-}]$$

There is more than one root to this equation so a bisection method is used to solve for $[H^+]$. This method involves setting an upper and lower bound for $[H^+]$ i.e. 10^{-1} and 10^{-14}. The calculated $[H^+]$ is used in the dissolution reactions of the next timestep. In the initial model timestep, $[H^+]$ is equal to the concentration in rainwater.

The original concentration of the oxide in the parent rock is calculated by

$$M_i = \mathrm{wt\%} \times \rho$$

where M_i is the concentration of oxide i ($g\,m^{-3}$), $wt\%$ is the original composition of oxide i in the parent rock and ρ is the density of the parent rock ($g\,m^{-3}$). At each timestep in the model, the suite of model equations calculates the proportion of the orginial oxide remaining in each soil layer. This value is used to calculate the new mole fraction of the oxide in the rock. For the model simulations in this study it is assumed that solutions are ideal and thus mole fraction is equal to activity. This activity value is used to calculate the new ion concentration at thermodynamic equilibrium using the above procedure.

A2 Mineralogy and Gibbs correction factors

To calculate the likely minerals present in the parent material from the bulk chemical analyses of the rock, the CIPW norm scheme is used. The CIPW method follows that of Hughes (1982). This method proceeds by expressing the oxides as molecular amounts and allocating the oxides to minerals in a step by step proceedure. For example, all P_2O_5 is used to make the mineral apatite which requires three times the amount of CaO, all TiO_2 is used to produce ilmenite using an equivalent amount of FeO, next all of K_2O is used to make orthoclase and all Na_2O is used to make albite unless there is not enough Al_2O_3, in which case the excess Na_2O is used to make acmite. The method continues in this nature until all oxides are allocated to minerals. Some of the allocations are then revised depending upon the saturation or undersaturation of silica. FeO and Fe_2O_3 are summed to give a total value for Fe and then a ratio of 0.1 Fe^{3+}/total Fe is applied. This is beacuse anomolously high Fe_2O_3 contents can be recorded if the rock has undergone post-crystallization oxidation (Hughes, 1982, pg. 97). The normative mineral assemblages obtained from the oxide compositions of Table A1 are shown in Table A2. This mineralogic configuration implies that the basalt is an alkali basalt where silica is undersaturated and nepheline is present. The correction factor for the ΔG_f for each oxide, λ, is found by comparing the free energies of these minerals with those of the constituent oxides and using the proportions of

these minerals present in the parent material to find the mean λ for each oxide. For the model simulations of this study TiO_2 is assumed to be insoluble.

A3 Hargreaves equation

$$\mathrm{PET} = 0.0023 \times R_a \times (T_{mean} + 17.8) \times \mathrm{TD}^{0.5} \quad \text{(A11)}$$

where PET is in units of $mm\,month^{-1}$. T_{mean} is the monthly mean temperature (°C), TD is the difference between the average monthly maximum and minimum temperatures (°C), R_a is the incoming extraterrestrial radiation ($mm\,day^{-1}$), this is calculated for the 15th day of the month. The monthly value is calculated by multiplying this daily value by the number of days in the month. Equation A12 estimates the extraterrestrial radiation using only latitude (ϕ) and the julian day (J) (Kouwen, 2010).

$$R_a = 15.392 \times d_r(w_s \times \sin\phi \times \sin\delta + \cos\phi \times \cos\delta \times \sin w_s) \quad \text{(A12)}$$

where d_r is the relative distance between the earth and the sun, given by

$$d_r = 1 + 0.033 \times \cos\left(\frac{2\pi J}{365}\right) \quad \text{(A13)}$$

δ is the solar declination (radians) defined by

$$\delta = 0.4093 \times \sin\left(\frac{2\pi J}{365} - 1.405\right) \quad \text{(A14)}$$

and w_s is the sunset hour angle (radians) given by

$$w_s = \arccos(-\tan\phi \times \tan\delta) \quad \text{(A15)}$$

A4 Calculating chemical weathering intensity

To quantify element losses due to chemical weathering only, mass balance techniques can be applied to soil profiles (April et al., 1986; Riebe et al., 2004a, b). When soluble elements leave soil profiles the immobile elements become enriched compared to their concentrations in the parent material. Therefore measurements of immobile element enrichment in soil profiles can be exploited to reveal the extent of chemical weathering losses of other elements in the profile (e.g. Taylor and Blum, 1995).

To calculate the depletion or accumulation of an element relative to its concentration in the bedrock the soil/rock ratios of the element are normalised with those of a known inert element such as Zirconium (Zr) or Titanium (Ti) (Brimhall and Dietrich, 1987). This ensures that the differences in element concentrations between bedrock and soil is due to chemical weathering only and not because of changes in the soil bulk density or due to losses of other elements.

The weathering intensity of elements in the Hawaiian soils are calculated by normalising them relative to Nb:

$$\tau_i = \frac{C_{i\mathrm{w}} \cdot \mathrm{Nb_p}}{C_{i\mathrm{p}} \cdot \mathrm{Nb_w}} \tag{A16}$$

where τ is the mass transfer coefficient of element i (Brimhall and Dietrich, 1987), p stands for the protolith or parent material, w is the weathered material or soil and C is the concentration of element i. $\tau_i = 1$ indicates that the element is enriched at the same ratio as Nb and is therefore immobile, $\tau_i = 0$ indicates complete depletion of element i and $\tau_i > 1$ represents relative enrichment of element i.

Acknowledgements. This work was funded by a NERC PhD stundentship awarded to MOJ. The authors are extremely grateful to Stephen Porder for generously publishing and making available the Hawaiian soil chronosequence data. We also thank Simon Mudd for providing comments on an earlier version of this paper.

References

April, R., Newton, R., and Truettner Coles, L.: Chemical weathering in two Adirondack watersheds: past and present-day rates, Geol. Soc. Am. Bull., 97, 1232–1238, 1986. 5843

Arora, V. K. and Boer, G. J.: A representation of variable root distribution in dynamic vegetation models, Earth Interact., 7, 1–19, 2003. 5819

Austin, A. T.: Differential effects of precipitation on production and decomposition along a rainfall gradient in Hawaii, Ecology, 83, 328–338, 2002. 5833

Berg, B. and McClaugherty, C.: Plant Litter, 2nd edn., Springer-Verlag, Berlin Heidelberg, Germany, 2008. 5825

Brimhall, G. H. and Dietrich, W. E.: Constitutive mass balance relations between chemical composition, volume, density, porosity, and strain in metasomatic hydrochemical systems: results on weathering and pedogenesis, Geochim. Cosmochim. Ac., 51, 567–587, 1987. 5834, 5843

Busacca, A. J. and Singer, M. J.: Pedogenesis of a chronosequence in the Sacramento Valley, California, USA., II. Elemental chemistry of silt fractions, Geoderma, 44, 43–75, 1989. 5828

Chadwick, O. A., Derry, L. A., Vitousek, P. M., Huebert, B. J., and Hedin, L. O.: Changing sources of nutrients during four million years of ecosystem development, Nature, 397, 491–497, 1999. 5813, 5832, 5835

Chadwick, O. A., Gavenda, R. T., Kelly, E. F., Ziegler, K., Olson, C. G., Elliott, W. C., and Hendricks, D. M.: The impact of climate on the biogeochemical functioning of volcanic soils, Chem. Geol., 202, 195–223, 2003. 5832

Chen, Z. and Wang, A. Y. X.: Effects of intergranular additions of oxides on the coercivity, thermal stability and microstructure of Nd-Fe-B magnets, J. Magn. Magn. Mater., 162, 307–313, 1996. 5853

Cohen, S., Willgoose, G., and Hancock, G.: The mARM3D spatially distributed soil evolution model: three-dimensional model framework and analysis of hillslope and landform reponses, J. Geophys. Res., 115, F04013, doi:10.1029/2009JF001536, 2010. 5813

Craig, H. and Poreda, R. J.: Cosmogenic ^{3}He in terrestrial rocks: the summit lavas of Maui, P. Natl. Acad. Sci. USA, 83, 1970–1974, 1986. 5833, 5851

Dietrich, W. E., Reiss, R., Hsu, M., and Montgomery, D. R.: A process-based model for colluvial soil depth and shallow landsliding using digital elevation data, Hydrol. Process., 9, 383–400, 1995. 5813

Finke, P. A. and Hutson, J. L.: Modelling soil genesis in calcareous loess, Geoderma, 145, 462–479, 2008. 5814
Gabet, E. J., Reichman, O. J., and Seabloom, E. W.: The effects of bioturbation on soil processes and sediment transport, Annu. Rev. Earth Pl. Sc., 31, 249–273, 2003. 5821
Garrels, R. M. and Christ, C. L.: Solutions, Minerals and Equilibria, Harper, New York, 1965. 5816
Goddéris, Y., Francois, L. M., Probst, A., Schott, J., Moncoulon, D., Labat, D., and Viville, D.: Modelling weathering processes at the catchment scale: the WITCH numerical model, Geochim. Cosmochim. Ac., 70, 1128–1147, 2006. 5814
Hargreaves, G. H. and Samani, Z. A.: Reference crop evapotranspiration from temperature, Appl. Eng. Agric., 1, 96–99, 1985. 5819
Haynes, W. M. and Lide, D. R. (Eds.): CRC Handbook of Chemistry and Physics: a Ready-Reference Book of Chemical and Physical Data, 91st edn., CRC: press, London, 2011. 5851
Hedin, L. O., Vitousek, P. M., and Matson, P. A.: Nutrient losses over four million years of tropical forest development, Ecology, 84, 2231–2255, 2003. 5832
Hillel, D.: Introduction to environmental soil physics, Elsevier Academic Press, San Diego, 2004. 5824
Hinsinger, P. and Jaillard, B.: Root-induced release of interlayer potassium and vermiculitization of phlogopite as related to potassium depletion in the rhizosphere of ryegrass, J. Soil Sci., 44, 525–534, 1993. 5835
Hinsinger, P., Elsass, F., Jaillard, B., and Robert, M.: Root-induced irreversible transformation of a trioctahedral mica in the rhizosphere of rape, J. Soil Sci., 44, 535–545, 1993. 5835
Hinsinger, P., Bengough, A. G., Vetterlein, D., and Young, I. M.: Rhizosphere: biophysics, biogeochemistry and ecological relevance, Plant Soil, 321, 117–152, 2009. 5834
Hoosbeek, M. R. and Bryant, R. B.: Towards the quantitative modeling of pedogenesis – a review, Geoderma, 55, 183–210, 1992. 5814
Hotchkiss, S., Vitousek, P. M., Chadwick, O. A., and Price, J.: Geomorphological change, and the interpretation of soil and ecosystem, Ecosystems, 3, 522–533, 2000. 5832
Hughes, C. J.: Igneous Petrology, Elsevier, Amsterdam, 1982. 5841
Humphreys, G. S. and Field, R.: Mixing, mounding and other aspects of bioturbation: implications for pedogenesis, in: 16th World Congress of Soil Science, International Society of Soil Science, Montpellier, Registered paper no. 18, 1998. 5821

Hutchens, E.: Microbial selectivity on mineral surfaces: possible implications for weathering processes, Fungal Biology Reviews, 2009, 115–121, 2009. 5834
Jackson, R. B., Canadell, J., Ehleringer, J. R., Mooney, H. A., Sala, O. E., and Schulze, E. D.: A global analysis of root distributions for terrestrial biomes, Oecologia, 108, 389–411, 1996. 5819, 5833, 5851
Jobbágy, E. G., and Jackson, R. B.: The distribution of soil nutrients with depth: Global patterns and the imprint of plants, Biogeochemistry, 53, 51–77, 2001. 5831, 5834
Johnson, M. O., Mudd, S. M., Pillans, B., Spooner, N. A., Fifield, L. K., Kirkby, M. J., and Gloor, M.: Quantifying the rate and depth dependence of bioturbation based on optically-stimulated luminescence (OSL) dates and meteoric 10-Be, Earth Surf. Proc., doi:10.1002/esp.3520, 2014. 5821, 5851
Jones, H. G.: Plants and Microclimate, Cambridge University Press, Cambridge, 1992. 5824, 5851
Kirkby, M. J.: Soil development models as a component of slope models, Earth Surf. Proc., 2, 203–230, 1977. 5815, 5816, 5817, 5853
Kirkby, M. J.: A basis for soil-profile modeling, J. Soil Sci., 36, 97–121, 1985. 5814, 5815, 5816, 5820, 5838, 5855
Knecht, M. F. and Goransson, A.: Terrestrial plants require nutrients in similar proportions, Tree Physiol., 24, 447–460, 2004. 5836
Kouwen, N.: WATFLOOD: Hydrological Model Routing and Flow Forcasting System, user Manual, 2010. 5842
Kurz, M. D.: In situ production of terrestrial cosmogenic helium and some applications to geochronology, Geochim. Cosmochim. Ac., 50, 2855–2862, 1986. 5833, 5851
Linder, S.: Analysis for detecting and correcting nutrient imbalances in Norway Spruce, Ecol. Bull., 44, 178–190, 1995. 5825
Lindsay, W. L.: Chemical Equilibria in Soils, John Wiley & Sons, New York, 1979. 5853, 5854
Lucas, Y.: The role of plants in controlling rates and products of weathering: importance of biological pumping, Annu. Rev. Earth Pl. Sc., 29, 135–163, 2001. 5826, 5831
Malhi, Y., Aragão, L. E. O. C., Metcalfe, D. B., Paiva, R., Quesada, C. A., Almeida, S., Anderson, L., Brando, P., Chambers, J. Q., Da Costa, A. C. L., Hutyra, L. R., Oliveira, P., Patiño, S., Pyle, E. H., Robertson, A. L., and Teixeira, L. M.: Comprehensive assessment of carbon productivity, allocation and storage in three Amazonian forests, Glob. Change Biol., 15, doi:10.1111/j.1365-2486.2008.01780.x, 2009. 5851, 5860

McBirney, A. R.: Igneous Petrology, 3rd edn., Jones and Bartlett Publishers, Boston, 2007. 5851
McGroddy, M. E., Daufresne, T., and Hedin, L. O.: Scaling of C : N : P stoichiometry in forests worldwide: implications of terrestrial Redfield-type ratios, Ecology, 85, 2390–2401, 2004. 5825
Minasny, B. and McBratney, A. B.: A rudimentary mechanistic model for soil production and landscape development, Geoderma, 90, 3–21, 1999. 5813
Minasny, B. and McBratney, A. B.: A rudimentary mechanistic model for soil formation and landscape development, II. A two-dimensional model incorporating chemical weathering, Geoderma, 103, 161–179, 2001. 5813
Minasny, B., McBratney, A. B., and Salvador-Blanes, S.: Quantitative models for pedogenesis – a review, Geoderma, 144, 140–157, 2008. 5814, 5837
Morton, K. W. and Mayers, D. F.: Numerical solution of partial differential equations, 2nd edn., Cambridge University Press, Cambridge, UK, 2005. 5826
Nesbitt, H. W. and Young, G. M.: Prediction of some weathering trends of plutonic and volcanic rocks based on thermodynamic and kinetic considerations, Geochim. Cosmochim. Ac., 48, 1523–1534, 1984. 5828
Nishiizumi, K., Klein, J., Middleton, R., and Craig, H.: Cosmogenic ^{10}Be, ^{26}Al, and ^{3}He in olivine from Maui lavas, Earth Planet. Sc. Lett., 98, 263–266, 1990. 5833, 5851
Parkhurst, D. L. and Appelo, C. A. J.: User's Guide to PHREEQC (Version 2) – A Computer Program for Speciation, Batch-Reaction, One-Dimensional Transport, and Inverse Geochemical Calculations, US Department of the interior, US Geological Survey, Denver, Colorado, Water Resources Investigations Report 99–4259, 1999. 5838
Penman, H. L.: Gas and vapour movements in the soil: I. the diffusion of vapours through porous solids, The Journal of Agricultural Society, 30, 437–462, 1940. 5824
Porder, S. and Chadwick, O. A.: Climate and soil-age constraints on nutrient uplift and retention by plants, Ecological Society of America, 90, 623–636, 2009. 5827, 5831, 5832, 5835, 5836, 5852
Porder, S., Hilley, G. E., and Chadwick, O. A.: Chemical weathering, mass loss, and dust inputs across a climate by time matrix in the Hawaiian Islands, Earth Planet. Sc. Lett., 258, 414–427, 2007. 5813, 5832, 5833, 5834, 5835
Quesada, C. A., Phillips, O. L., Schwarz, M., Czimczik, C. I., Baker, T. R., Patiño, S., Fyllas, N. M., Hodnett, M. G., Herrera, R., Almeida, S., Alvarez Dávila, E., Arneth, A., Arroyo, L., Chao, K. J., Dezzeo, N., Erwin, T., di Fiore, A., Higuchi, N., Honorio Coronado, E., Jimenez, E. M., Killeen, T., Lezama, A. T., Lloyd, G., López-González, G., Luizão, F. J., Malhi, Y., Monteagudo, A., Neill, D. A., Núñez Vargas, P., Paiva, R., Peacock, J., Peñuela, M. C., Peña Cruz, A., Pitman, N., Priante Filho, N., Prieto, A., Ramírez, H., Rudas, A., Salomão, R., Santos, A. J. B., Schmerler, J., Silva, N., Silveira, M., Vásquez, R., Vieira, I., Terborgh, J., and Lloyd, J.: Basin-wide variations in Amazon forest structure and function are mediated by both soils and climate, Biogeosciences, 9, 2203–2246, doi:10.5194/bg-9-2203-2012, 2012. 5813
Raich, J. W.: Aboveground productivity and soil respiration in three Hawaiian rain forests, Forest Ecol. Manag., 107, 309–318, 1998. 5863
Riebe, C. S., Kirchner, J., and Finkel, R.: Sharp decrease in long-term chemical weathering rates along an altitudinal transect, Earth Planet. Sc. Lett., 218, 421–434, 2004a. 5843
Riebe, C. S., Kirchner, J. W., and Finkel, R. C.: Erosional and climatic effects on long-term chemical weathering rates in granitic landscapes spanning diverse climatic regimes, Earth Planet. Sc. Lett., 224, 547–562, 2004b. 5843
Salvador-Blanes, S., Minasny, B., and McBratney, A.: Modelling long-term in situ soil profile evolution: application to the genesis of soil profiles containing stone layers, Eur. J. Soil Sci., 58, 1535–1548, 2007. 5813
Sander, H.: The porosity of tropical soils and implications for geomorphological and pedogenetic processes and the movement of solutions within the weathering cover, Catena, 42, 129–137, 2002. 5838
Schuur, A. G. and Matson, P. A.: Net primary productivity and nutrient cycling across a mesic to wet precipitation gradient in Hawaiian montane forest, Oecologia, 128, 431–442, 2001. 5833, 5863
Tardy, Y., Bocquier, G., Paquet, H., and Millot, G.: Formation of clay from granite and its distribution in relation to climate and topography, Geoderma, 10, 271–284, 1973. 5829
Taylor, A. and Blum, J. D.: Relation between soil age and silicate weathering rates determined from the chemical evolution of a glacial chronosequence, Geology, 23, 979–982, 1995. 5843
Townsend, A. R., Vitousek, P. M., and Trumbore, S. E.: Soil organic matter dynamics along gradients in temperature and land use on the island of Hawaii, Ecology, 76, 721–733, 1995. 5833, 5863

Trumbore, S. E., Davidson, E. A., Barbosa de Camargo, P., Nepstad, D. C., and Martinelli, A. L.: Belowground cycling of carbon in forests and pastures of Eastern Amazonia, Global Biogeochem. Cy., 9, 515–528, 1995. 5823

Urey, H. C.: The planets: their origin and development, Yale University Press, New Haven, Connecticut, 1952. 5813

Van Dam, D., Veldkamp, E., and Van Breemen, N.: Soil organic carbon dynamics: variability with depth in forested and deforested soils under pasture in Costa Rica, Biogeochemistry, 39, 343–375, 1997. 5823

Vanwalleghem, T., Stockmann, U., Minasny, B., and McBratney, A. B.: A quantitative model for integrating landscape evolution and soil formation, J. Geophys. Res.-Ea. Surf., 118, 331–347, 2013. 5813

Veldkamp, E.: Organic-carbon turnover in three tropical soils under pasture after deforestation, Soil Sci. Soc. Am. J., 58, 175–180, 1994. 5823

Vitousek, P. M. and Farrington, H.: Nutrient limitation and soil development: experimental test of a biogeochemical theory, Biogeochemistry, 37, 63–75, 1997. 5832

Vitousek, P. M. and Sanford Jr, R. L.: Nutrient cycling in moist tropical forest, Annu. Rev. Ecol. Syst., 17, 137–167, 1986. 5813

Vitousek, P. M., Walker, L. R., Whiteaker, L. D., and Matson, P. A.: Nutrient limitations to plant growth during primary succession in Hawaii Volcanoes National Park, Biogeochemistry, 23, 197–215, 1993. 5813

Vitousek, P. M., Turner, D. R., Parton, W. J., and Sanford, R. L.: Litter decomposition on the Mauna Loa environmental matrix, Hawai'i: patterns, mechanisms and models, Ecology, 75, 418–429, 1994. 5832

von Blackenburg, F.: The control mechanisms of erosion and weathering at basin scale from cosmogenic nuclides in river sediment, Earth Planet. Sc. Lett., 237, 462–479, 2005. 5833

Walker, J. C. G., Hays, P. B., and Kasting, J. F.: A negative feedback mechanism for the long-term stabilization of Earth's surface temperature, J. Geophys. Res., 86, 9776–9782, 1981. 5813

Wallman, P., Svensson, M. G. E., Sverdrup, H., and Belyazid, S.: For SAFE – an integrated process-orientated forest model for long-term sustainability assessments, Forest Ecol. Manag., 207, 19–36, 2005. 5814

Warfvinge, P. and Sverdrup, H.: Calculating critical loads of acid deposition with PROFILE – a steady-state soil chemistry model, Water Air Soil Poll., 63, 119–143, 1992. 5814

White, A. F., Bullen, T. D., Schulz, M. S., Blum, A. E., Huntington, T. G., and Peters, N. E.: Differential rates of feldspar weathering in granitic regoliths, Geochim. Cosmochim. Ac., 65, 847–869, 2001. 5816, 5828

White, A. F., Schulz, M. S., Vivit, D. V., Blum, A. E., Stonestrom, D. A., and Anderson, S. P.: Chemical weathering of a marine terrace chronosequence, Santa Cruz, California I: Interpreting rates and controls based on soil concentration-depth profiles, Geochim. Cosmochim. Ac., 72, 36–68, 2008. 5816, 5828

Wilkinson, M. T. and Humphreys, G. S.: Exploring pedogenesis via nuclide-based soil production rates and OSL-based bioturbation rates, Aust. J. Soil Res., 43, 767–779, 2005. 5821, 5822

Yoo, K. and Mudd, S. M.: Toward process-based modeling of geochemical soil formation across diverse landforms: a new mathematical framework, Geoderma, 146, 248–260, 2008. 5813

Yoo, K., Amundson, R., Heimsath, A. M., and Dietrich, W. E.: Process-based model linking pocket gopher (*Thomomys bottae*) activity to sediment transport and soil thickness, Geology, 33, 917–920, 2005. 5821

Table 1. Model parameters

Parameter	Value	Unit	Description	Source
$\frac{d}{dx}(Kg)$	2	yr^{-1}	Hydraulic conductivity and gradient	This study
F_0	0.05	$m\,yr^{-1}$	Rate of percolation into bedrock	This study
D_l	1×10^{-2}	$m^2\,yr^{-1}$	Diffusion coefficient for ionic diffusion	Haynes and Lide (2011)
D	2×10^{-4}	$m^2\,yr^{-1}$	Diffusion coefficient for bioturbation	Johnson et al. (2014)
z_b	0.28	m	e-folding length scale for biouturbation	Johnson et al. (2014)
T	6	$\mu m\,yr^{-1}$	Denudation rate	Craig and Poreda (1986); Kurz (1986); Nishiizumi et al. (1990)
z_r	0.26	m	e-folding length scale for root distribution	Jackson et al. (1996)
N_P	1.0	$kg\,m^{-2}\,yr^{-1}$	Net productivity of carbon	Malhi et al. (2009)
k_{fine}	1	yr^{-1}	Decay coefficient of fine litter and roots	This study
k_{coarse}	0.02	yr^{-1}	Decay coefficient of coarse litter and roots	This study
α_1	0.21	–	Proportion of N_P allocated to fine roots	Malhi et al. (2009)
α_2	0.08	–	Proportion of N_P allocated to coarse roots	Malhi et al. (2009)
α_3	0.36	–	Proportion of N_P allocated to fine litter	Malhi et al. (2009)
α_4	0.36	–	Proportion of N_P allocated to coarse litter	Malhi et al. (2009)
fN_{Pl}	0.62	%	Percentage of fine leaf biomass production allocated to nutrients	This study
fN_{Pr}	0.2	%	Percentage of fine root biomass production allocated to nutrients	This study
R_c	0.56	$kg\,C\,m^{-2}\,yr^{-1}$	CO_2 production from root respiration	Malhi et al. (2009)
z_k	0.26	m	e-folding length scale for carbon decay coefficients	This study
D_c	14.7	$mm^2\,s^{-1}$	Diffusion coefficient for gaseous mixing	Jones (1992)
$\rho_{bedrock}$	3.01	$g\,cm^{-3}$	Bedrock density	McBirney (2007)

Table 2. Composition (wt%) of three laval flows taken from Porder and Chadwick (2009)

Flow	SiO_2	Al_2O_3	Fe_2O_3	CaO	MgO	Na_2O	K_2O	TiO_2	P_2O_5
Kona (10 ka)	45.5	9.0	13.3	7.4	18.7	1.4	0.2	1.6	0.1
Hawi (170 ka)	45.5	18.4	12.4	4.8	3.0	4.1	1.6	2.6	1.6
Pololu (350 ka)	47.4	14.4	13.7	10.0	6.9	2.7	0.9	3.2	0.5

Table A1. Oxide composition of a basalt and ΔG_f values for the rock oxides

Oxide	wt %	ΔG_f (kcal mol^{-1})
SiO_2	45.5	−204.66[a]
Al_2O_3	9.0	−378.18[a]
Fe_2O_3	1.3	−177.85[b]
MgO	18.7	−142.52[a]
CaO	7.4	−144.19[a]
Na_2O	1.4	−89.74[a]
K_2O	0.2	−76.76[c]
TiO_2	1.6	−212.43[a]
FeO	12.0	−58.68[b]
P_2O_5	0.1	−644.80[d]

[a] Haynes and Lide (2011).
[b] Lindsay (1979).
[c] Kirkby (1977).
[d] Chen and Wang (1996).

Table A2. CIPW normative mineral assemblage of basalt.

Mineral	Formula	Wt%	ΔG_f (kcal mol^{-1})[a]
Quartz	SiO_2	0	−204.66
Corundum	Al_2O_3	0	−378.18
Anorthite	$CaAl_2Si_2O_8$	18.18	−960.68
Diopside	$MgCaSi_2O_6$	15.25	−724.62
Hypersthene	$MgSiO_3$	12.94	−349.41 (enstatite)
	$FeSiO_3$	5.07	−257.60 (ferrosilite)
Albite	$NaAlSi_3O_8$	12.18	−887.41
Orthoclase	$KAlSi_3O_8$	1.21	−894.71
Olivine	Mg_2SiO_4	22.93	−491.30 (forsterite)
	Fe_2SiO_4	6.83	−329.31 (fayalite)
Nepheline	$NaAlSiO_4$	0	−477.24
Leucite	$KAlSi_2O_6$	0	−687.62
Apatite	$Ca_{10}(PO_4)_6F$	0.22	−3094.73
Ilmenite	$FeTiO_3$	3.12	–
Magnetite	Fe_3O_4	1.98	−243.47
Hematite	Fe_2O_3	0	−177.85

[a] Lindsay (1979).

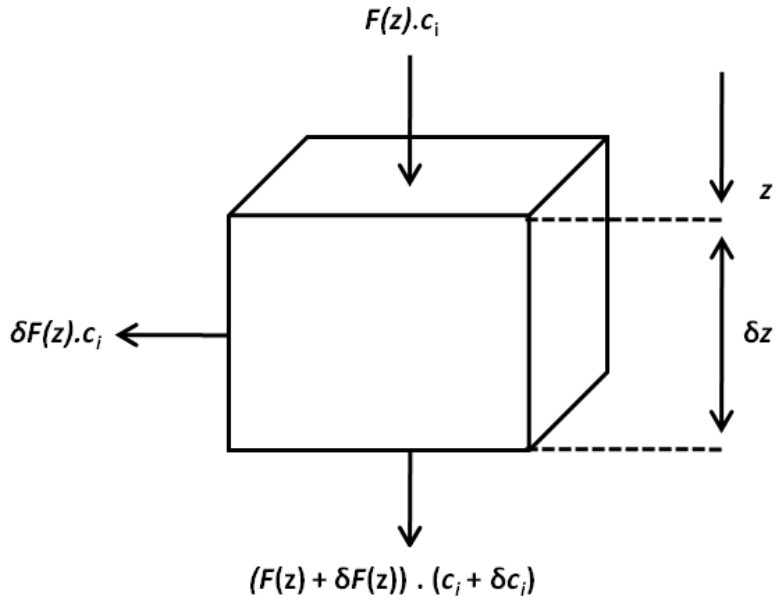

Fig. 1. Schematic overview of solute mass balance where F is the rate of percolation ($m yr^{-1}$) at depth z and c is the concentration of ion i in solution ($g m^{-3}$). Adapted from Kirkby (1985)

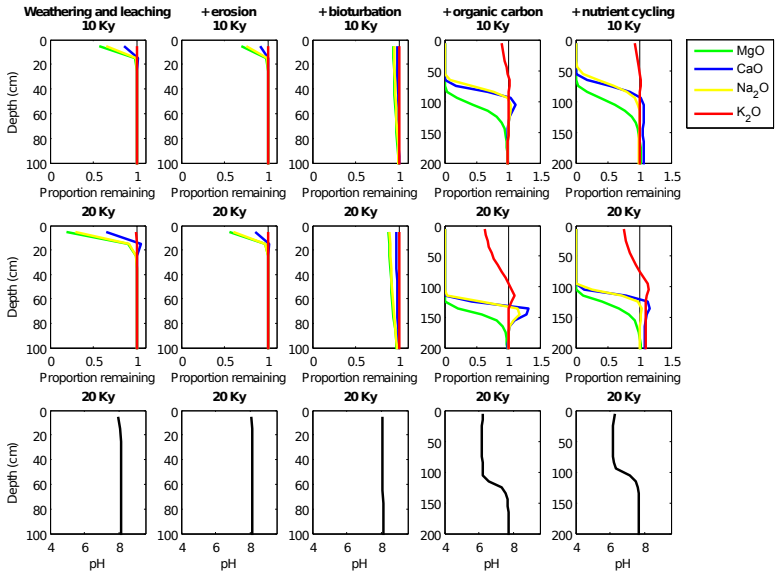

Fig. 2. Vertical distributions of pH and the relative depletion/enrichment of the basic model oxides over 20 ka of soil development for five different model runs of increasing complexity. Values < 1 indicate a loss relative to the parent material, and values > 1 indicate relative accumulation.

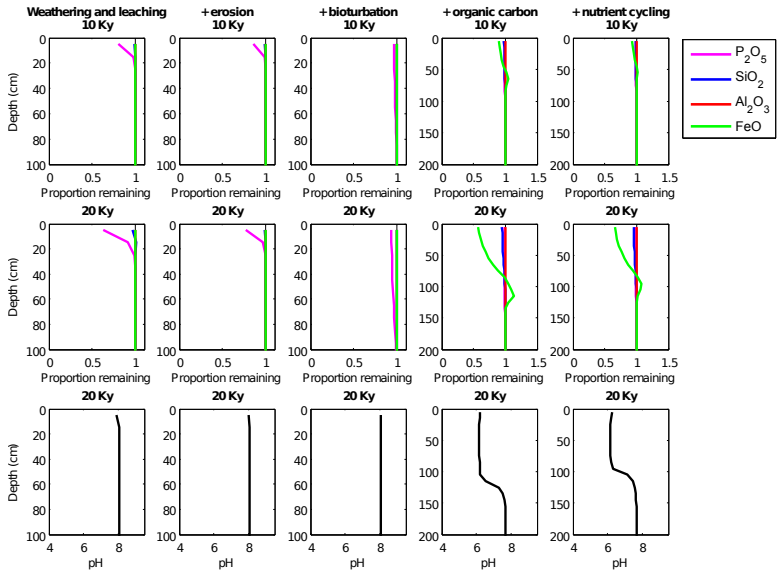

Fig. 3. Vertical distributions of pH the relative depletion/enrichment of the non-basic model oxides over 20 ka of soil development for five different model runs of increasing complexity. Values < 1 indicate a loss relative to the parent material, and values > 1 indicate relative accumulation.

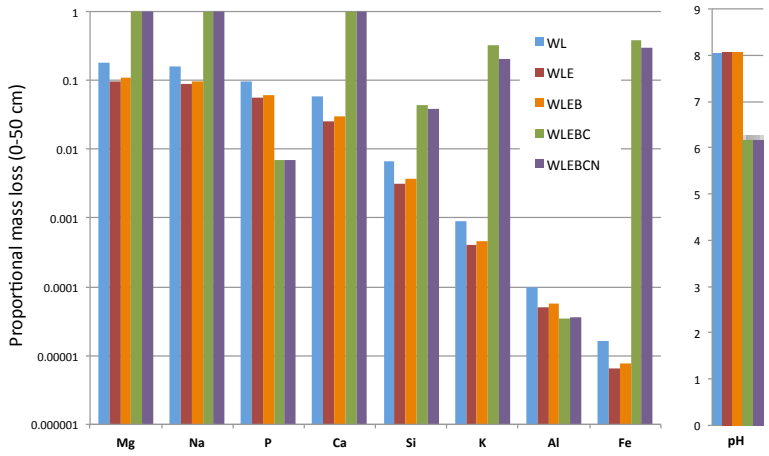

Fig. 4. Proportional mass loss of each model element relative to the amount in the parent material and mean pH for the top 50 cm of the soil profile after 20 ka of soil development for each of the model simulations (WL = weathering and leaching, E = erosion, B = bioturbation, C = organic carbon and N = nutrient cycling).

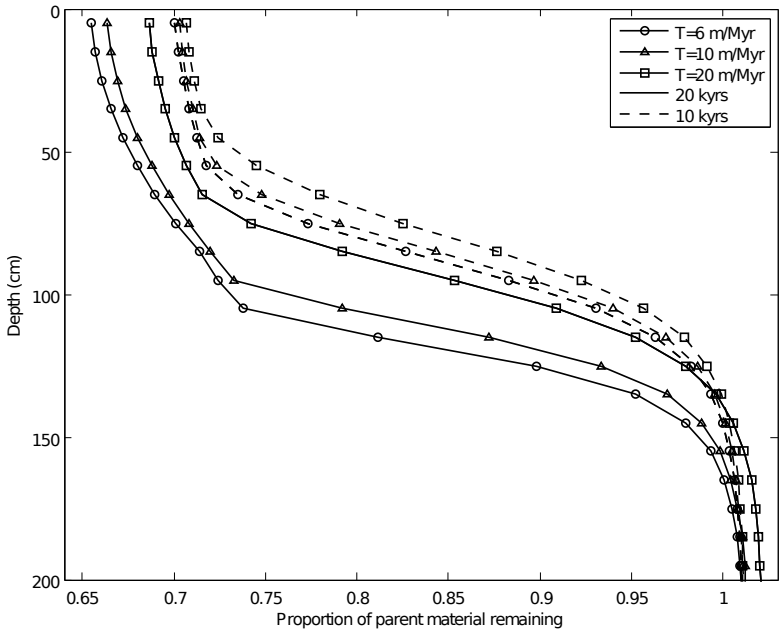

Fig. 5. Proportion of original parent material remaining after 10 and 20 ka of model simulation for 3 different rates of surface erosion (T).

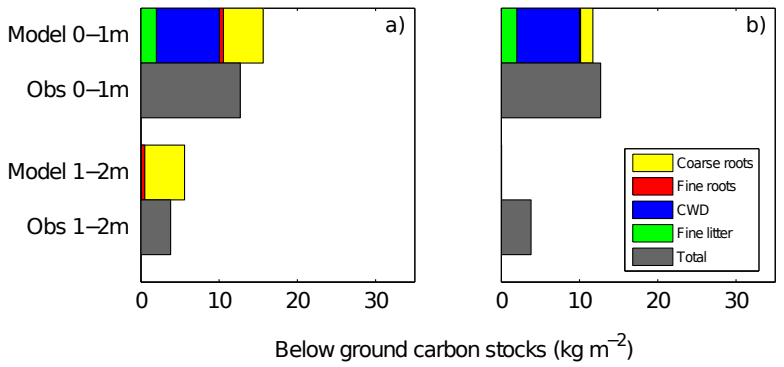

Fig. 6. Steady-state distribution of organic carbon pools for **(a)** the control run (Table 1) and **(b)** a constant decay rate with soil depth. Observations are from the Manaus site in Malhi et al. (2009). The total N_P for both runs is the same as the previous simulations which is equal to that estimated by Malhi et al. (2009) for the Manaus forest plot (Table 1).

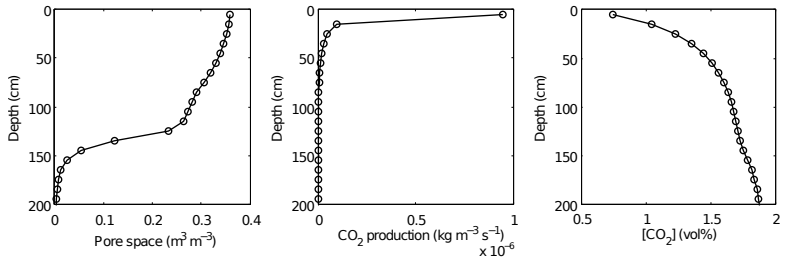

Fig. 7. Profiles of pore space (1-p), CO_2 production rate and CO_2 concentration after 20 ka of soil development.

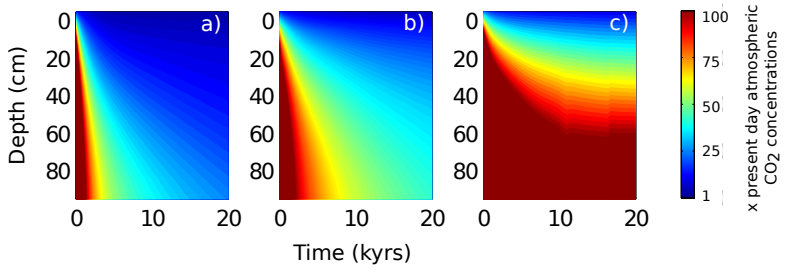

Fig. 8. Evolution of CO_2 profiles over 20 ka of soil development for three different model scenarios. $N_P = 0.5\,kg\,m^{-2}\,yr^{-1}$ and $z_r = 0.26$ **(a)**, $N_P = 1\,kg\,m^{-2}\,yr^{-1}$ and $z_r = 0.26$ **(b)** and $N_P = 1\,kg\,m^{-2}\,yr^{-1}$ and $z_r = 0.5$ **(c)**.

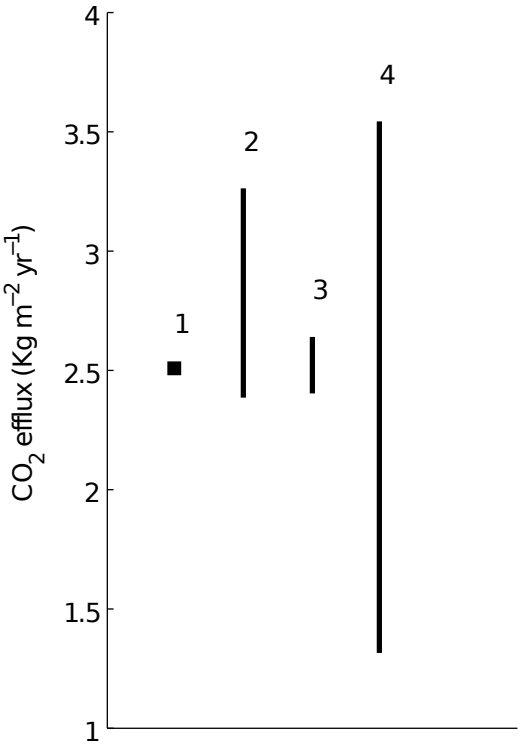

Fig. 9. Modelled soil respiration rate after 20 ka of soil development (1) and ranges of measured soil respiration rates from the following studies of Hawaiian tropical soils (2) Raich (1998) (3) Townsend et al. (1995) (4) Schuur and Matson (2001).

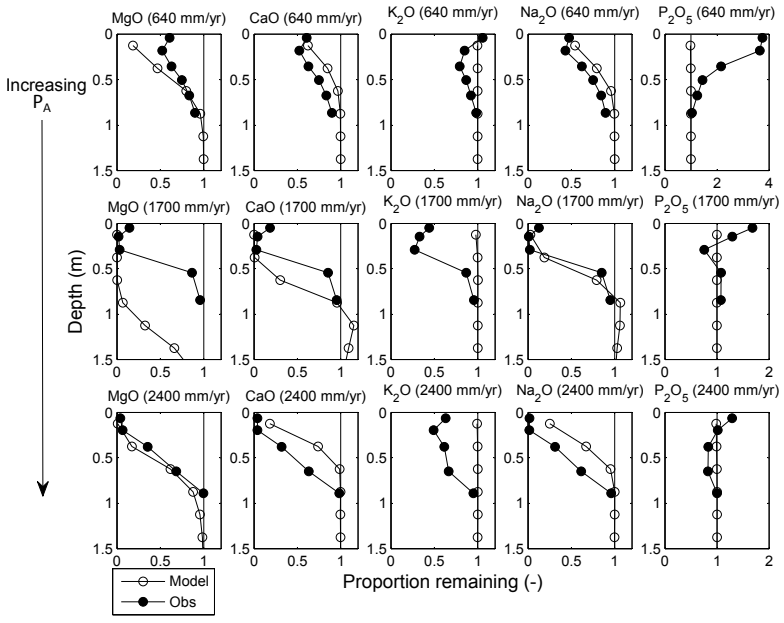

Fig. 10. Observed vs. simulated oxide losses/gains across a mean annual precipitation gradient (P_A) on the 10 ka Kona lava flow. Values < 1 indicate a loss relative to the parent material, and values > 1 indicate relative accumulation.

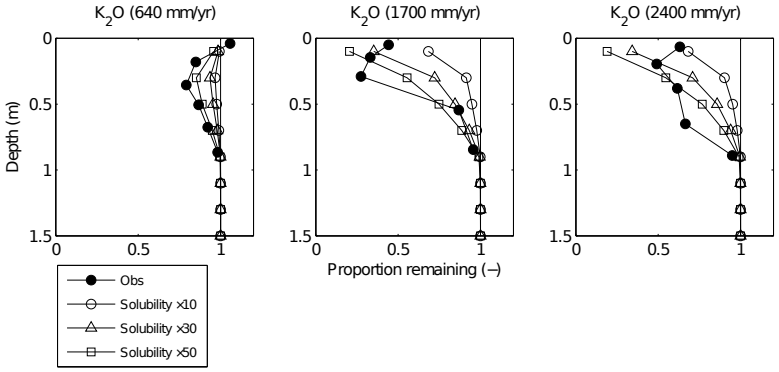

Fig. 11. Observed vs. simulated K for the 10 ka Kona flow for 3 different simulations of increased K solubility.

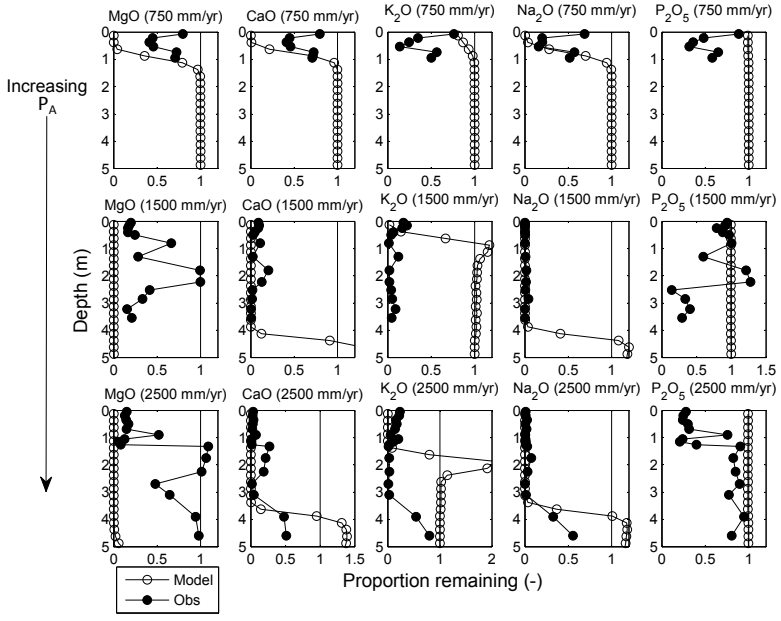

Fig. 12. Observed vs. simulated oxide losses/gains across a mean annual precipitation gradient (P_A) on the 170 ka Hawi lava flow. Values < 1 indicate a loss relative to the parent material, and values > 1 indicate relative accumulation.

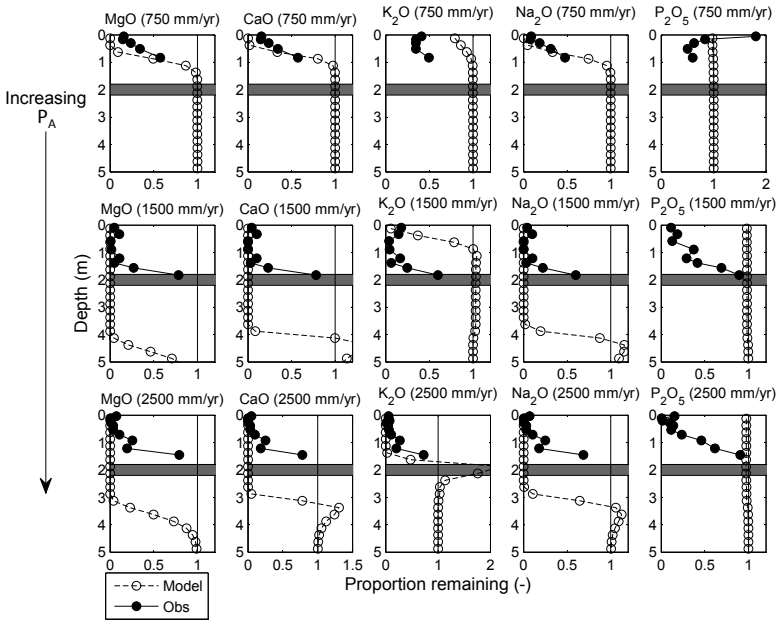

Fig. 13. Observed vs. simulated oxide losses/gains across a mean annual precipitation gradient (P_A) on the 350 ka Pololu lava flow. Values < 1 indicate a loss relative to the parent material, and values > 1 indicate relative accumulation. The grey box shows the location of the pahoehoe flow.

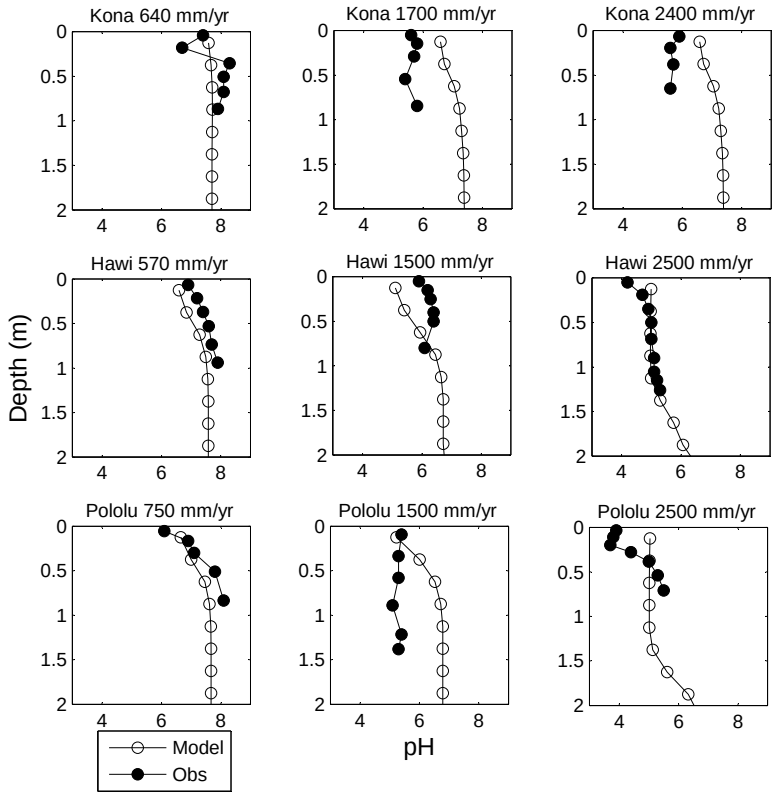

Fig. 14. Observed vs. simulated pH for 3 sites on each of the lava flows.